BEYOND TWO-EQUATION TURBULENCE MODELING FOR THE REYNOLDS-AVERAGED NAVIER-STOKES EQUATIONS: ADVANCES IN COMPLEX FLOW PREDICTIONS

David D. Marshall* , Travis M. Storm**
*ddmarsha@calpoly.edu, Associate Professor, California Polytechnic State University, San Luis Obispo, CA 93407-0352
**Former Graduate Student, California Polytechnic State University, San Luis Obispo, CA 93407-0352

Keywords: *Turbulence Models, RANS, $v^2 - f$*

Abstract

This paper explores the applicability of linear and nonlinear $v^2 - f$ turbulence models to circulation control flows. The model constants have been calibrated using on a flat plate and a two-dimensional hill. These models were applied to the General Aviation Circulation Control airfoil to assess the applicability of the models to circulation control flows. The results indicate that the $v^2 - f$ turbulence models perform better at predicting the lift, but it did not adequately capture the local flow properties.

1 General Introduction

To generate increased lift from traditional subsonic airfoils, either the angle of attack or the camber must be increased. The maximum lift coefficient of a traditional wing is limited by the eventual separation of flow over the wing, due primarily to the adverse pressure gradient that builds on the wing as lift is increased. Traditionally, this obstacle is overcome by use of complex moving wing surfaces, including flaps, slats, and other devices.

Circulation control has been proposed as a simpler and more effective alternative to the usual high-lift devices [1]. Circulation control is an active flow control device that increases the lift coefficient without the use of complex components in freestream flow. Circulation control is primarily needed when high lift coefficients are required due to low airspeeds, particularly during takeoff and landing. The technology makes use of the Coanda effect, according to which a fluid has a tendency to stay attached to an adjacent curved surface [2]. A high-speed jet of air is blown out of the leading and/or trailing edge of a wing, which follows the wing surface. The stagnation point on the leading edge and the flow separation point on the trailing edge are thus manipulated such that the circulation is increased, and consequently lift is increased.

The extent of the stagnation and separation point movement is primarily a function of the jet momentum coefficient, C_μ. The jet momentum coefficient is a measure of the jet momentum relative to the freestream momentum, and has two common formulations, which are defined as follows

$$C_\mu = \left(\frac{2h_{\text{jet}} b_{\text{jet}}}{S} \right) \left(\frac{\rho_{\text{jet}}}{\rho_\infty} \right) \left(\frac{U_{\text{jet}}^2}{U_\infty^2} \right) \quad (1)$$

$$= \frac{\dot{m} U_{\text{jet}}}{q_\infty S} \quad (2)$$

Traditional CFD approaches have been applied to circulation control airfoils, mostly in two dimensions, with mixed success. Unfortunately, the physics of circulation control wings are highly complex, and are not well understood due to limited experimental studies. The high momentum of the circulation control jet allows the boundary layer to remain attached longer than usual, thereby moving the separation point. This movement of the separation point is the primary reason that lift is augmented, and any CFD modeling techniques must be able to accurately model the separation point by properly predicting the spreading rate of the jet and the exchange of momentum between the jet and the surrounding fluid.

Todays computer resources limit most academic and industrial CFD to RANS solutions, especially for high Reynolds number flows. Many attempts have been made to model circulation control flow fields using common turbulence models (including Baldwin-Lomax [3, 4, 5], Spalart-Allmaras [1, 4, 5, 6, 7, 8, 9], $k-\epsilon$ [10], and $k-\omega$ [8, 9, 10, 11]) and while acceptable accuracy has been obtained in some cases, the general consensus has been that these models are not well suited for circulation control flow fields.

2 Summary of Turbulence Models Used

The traditional approach relating the Reynolds stresses to the mean strain rate tensor has been to make use of the Boussinesq assumption, where the turbulent viscosity creates a linear relationship between the Reynolds stresses and the mean strain rate tensor. Equation (3) shows this relationship.

$$\overline{\rho u_i'' u_j''} = \frac{2}{3}\rho k \delta_{ij} - 2\mu_t S_{ij} \qquad (3)$$

$$\text{with} \quad S_{ij} = \frac{1}{2}\left(\frac{\partial u_i}{\partial x_j} + \frac{\partial u_j}{\partial x_i}\right)$$

where $\overline{\rho u_i'' u_j''}$ is the Reynolds stress tensor, S_{ij} is the mean strain rate tensor, k is the tur-

bulence kinetic energy and μ_t is the turbulent eddy viscosity.

Common linear eddy viscosity formulations can vary in complexity from zero-equation (algebraic) to four-equation; the number of equations refers to the number of differential equations that need to be solved in a given model. Examples of zero-equation linear eddy viscosity models include the Cebeci-Smith [12] and Baldwin-Lomax [13] models. The most common one-equation model is the Spalart-Allmaras turbulence model [14]. Two-equation models include the $k-\epsilon$ models [15] and the $k-\omega$ model [16] turbulence models. The standard $v^2 - f$ turbulence model [17] is an increasingly common four-equation turbulence model.

Linear eddy viscosity models have proven to be quite powerful in CFD applications, but the linearization of the relationship between the Reynolds stresses and the strain rate can cause these models to produce non-physical results. In particular, the Boussinesq assumption results in isotropic normal viscous stresses, i.e.

$$\overline{\rho u''\,^2} = \overline{\rho v''\,^2} = \overline{\rho w''\,^2} = \frac{2}{3}\rho k \qquad (4)$$

Thus, any anisotropy in the Reynolds stresses (such as near-wall anisotropy) cannot be captured.

One approach to solving this shortcoming has been to introduce empirical damping functions or other sorts of ad-hoc modifications. This allows improvement upon a model for a given type of flow, but is far from universal. Pope [18] suggested that the more robust approach to this problem is to reformulate the relationship between the Reynolds stresses and the strain rate in a nonlinear manner. The general approach to formulating a nonlinear eddy viscosity model is to generalize the formulation of the Reynolds stresses to the following

$$\overline{\rho u_i'' u_j''} = \frac{2}{3}\rho k \delta_{ij} + \rho k \sum_{\lambda} g^{\lambda} T_{ij}^{\lambda} \qquad (5)$$

where T_{ij}^{λ} are the tensor bases and g^{λ} are the calibrated expansion coefficients. The specific approach to deriving the general form of the Reynolds stresses can vary depending on the number and form of the terms chosen to include in the tensor bases.

2.1 Standard Turbulence Models

For this work, the standard one-equation turbulence Spalart-Allmaras model [14] and the standard two-equation $k-\epsilon$ [15] and $k-\omega$ [16] models are used within FLUENT.

2.2 $v^2 - f$ with Linear Eddy Viscosity

Durbin [17] developed the $v^2 - f$ turbulence model to be used in flows in which near-wall turbulence is of significant importance, specifically flows with separation, recirculation, or heat transfer [19]. The model solves four transport equations, those for turbulence kinetic energy, turbulence dissipation rate, velocity scale, and an elliptic relaxation factor. The model is essentially an extension of the $k - \epsilon$ turbulence model, with the computational advantage of using the eddy viscosity concept to close the transport equations (as opposed to full second moment closure), but improves upon several known deficiencies of the $k-\epsilon$ model. Specifically, the $v^2 - f$ model can be integrated to a solid wall, eliminating the need for damping functions or wall functions [20]. Also, the introduction of the velocity scale allows the model to correctly scale damping of turbulence transport near walls, which turbulence kinetic energy cannot do [21]. In recent years, the $v^2 - f$ turbulence model has proven robust and superior to other RANS methods, despite its linear eddy viscosity formulation and insensitivity to streamline curvature [19].

The $v^2 - f$ turbulence model uses the same transport equations for turbulence kinetic energy and turbulence dissipation rate as does the $k - \epsilon$ turbulence model. In addition to these transport equations, this model solves the following transport equations for the ve-

locity scale and the elliptic relaxation factor. These four transport equations are

$$\frac{\partial}{\partial t}(\rho k) + \frac{\partial}{\partial x_j}(\rho k u_j)$$
$$= P_k - \rho \epsilon$$
$$+ \frac{\partial}{\partial x_j}\left[\left(\mu + \frac{\mu_t}{\sigma_k}\right)\frac{\partial k}{\partial x_j}\right] \quad (6)$$

$$\frac{\partial}{\partial t}(\rho \epsilon) + \frac{\partial}{\partial x_j}(\rho \epsilon u_j)$$
$$= \frac{C_{\epsilon 1}^* P_k - \rho C_{\epsilon 2}\epsilon}{T}$$
$$+ \frac{\partial}{\partial x_j}\left[\left(\mu + \frac{\mu_t}{\sigma_\epsilon}\right)\frac{\partial \epsilon}{\partial x_j}\right] \quad (7)$$

$$\frac{\partial}{\partial t}\left(\rho\overline{v^2}\right) + \frac{\partial}{\partial x_j}\left(\rho\overline{v^2}u_j\right)$$
$$= \rho k f - 6\rho\overline{v^2}\frac{\epsilon}{k}$$
$$+ \frac{\partial}{\partial x_j}\left[\left(\mu + \frac{\mu_t}{\sigma_k}\right)\frac{\partial\overline{v^2}}{\partial x_j}\right] \quad (8)$$

$$L^2\frac{\partial f^2}{\partial x_j} - f$$
$$= \frac{C_1 - 1}{T}\left(\frac{\overline{v^2}}{k} - \frac{2}{3}\right) - C_2\frac{P_k}{\rho k} \quad (9)$$

where P_k represents the production of turbulence kinetic energy due to the mean flow velocity gradients and is modeled as

$$P_k = 2\mu_t S_{ik}S_{ik} \quad (10)$$

The turbulence length scale, L, and the turbulence time scale, T, are represented as

$$L = C_L \max\left[\frac{k^{3/2}}{\epsilon}, C_\eta\left(\frac{\mu^3}{\rho^3\epsilon}\right)^{1/4}\right] \quad (11)$$

$$T = \max\left(\frac{k}{\epsilon}, C_T\sqrt{\frac{\mu}{\rho\epsilon}}\right) \quad (12)$$

Finally, the turbulent viscosity is obtained from

$$\mu_t = \rho C_\mu\overline{v^2}T \quad (13)$$

It is important to note that this model does not use any wall functions or turbulence damping functions. Instead, the model uses the ve-

locity scale (which is a measure of velocity fluctuation normal to streamlines) to damp turbulence transport near inhomogeneities, and the elliptic relaxation function to model non-local effects.

2.3 $v^2 - f$ with Nonlinear Eddy Viscosity

One deficiency in the standard $v^2 - f$ turbulence model is the use of the Boussinesq assumption to linearize the relationship between the Reynolds stresses and the mean strain rate. Pettersson Reif [22] proposed a nonlinear constitutive relationship that could account for turbulence anisotropy, thereby improving the $v^2 - f$ predictive capability of the turbulence model for turbulent shear flows. The nonlinearization begins with the proposal by Pope [18] for an equilibrium solution of a second-moment closure. The resulting formulation is

$$\overline{\rho u_i'' u_j''} = \frac{2}{3}\rho k \delta_{ij} - 2\rho C_\mu \overline{v^2} \tau_1 S_{ij}$$
$$+ \rho V \tau^2 C_{\mu 3} \left(S_{ik} S_{kj} - \frac{1}{3} S^2 \delta_{ij} \right) \quad (14)$$

where the coefficients are defined as

$$S^2 = S_{kl} S_{kl} \quad (15)$$

$$C_{\mu 3} = \frac{6}{5} \left(\frac{1}{\gamma_1 + \eta_1} \right) \quad (16)$$

$$\eta_1 = \tau^2 S_{ij} S_{ij} \quad (17)$$

$$\gamma_1 = \frac{1}{0.1 + \eta_1} \quad (18)$$

$$V = \max \left(\frac{2}{3} - \frac{\overline{v^2}}{k}, 0 \right) \quad (19)$$

Details of the development of this model can be found in [23].

2.4 FLUENT Integration

The above $v^2 - f$ turbulence models were written as user-defined functions used within the commercial CFD solver FLUENT. These models were based on the work of Herschl et al. [24, 25] with the addition of stability and robustness improvements.

3 Validation Cases

Two validation cases are presented here that were used to calibrate and validate the turbulence models. Details of the calibration process can be found in [23].

3.1 Flat Plate

The first validation case is the standard incompressible, turbulent flat plate. The constants used in the $v^2 - f$ turbulence model have been altered and calibrated numerous times since the model was first introduced. Many authors make logical arguments for the order of magnitude of the contents, but the constants have no universally accepted values. To address this issue, the constants were calibrated for a turbulent flow over a flat plate. Particular attention was paid to two aspects of the flat plate flow. First, the skin friction profile needed to match the well-known experimental profile from [26]

$$C_f = \frac{0.027}{\text{Re}_x^{1/7}} \quad (20)$$

Second, the model was tuned such that the near-wall velocity profile matched the widely accepted velocity profile throughout the turbulent boundary layer.

for $y^+ < 5$
$$u^+ = y^+ \quad (21)$$
for $5 \leq y^+ < 30$
$$u^+ = -y^+$$
$$+ e^{-\kappa B} \left[e^{\kappa u^+} - 1 - \kappa u^+ \right.$$
$$\left. -\frac{1}{2} \left(\kappa u^+ \right)^2 - \frac{1}{6} \left(\kappa u^+ \right)^3 \right] \quad (22)$$
for $30 \leq y^+ < 350$
$$u^+ = \frac{1}{\kappa} \ln \left(u^+ \right) + B \quad (23)$$

Figure 1 shows the skin friction coefficient results for several turbulence models including

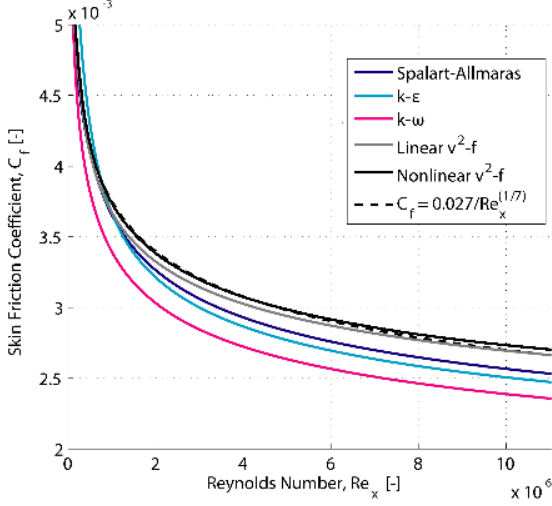**Fig. 1** Turbulent flat plate skin friction co-efficients for the turbulence models and the experimental curve fit from White [26].

Fig. 2 Turbulent flat plate velocity profiles for the turbulence models and the experimental data from Wieghardt [27].

the newly implemented linear $v^2 - f$ and non-linear $v^2 - f$ models. These new models were calibrated to best match skin friction curve from [26].

Figure 2 shows the velocity profile through the boundary layer for the two new turbulence model implementations. These models were calibrated to best fit the experimental data from [27]. The turbulence models capture the entire velocity profile.

3.2 S3H4 2D Hill

The flow over a 2D sinusoidal hill was used as a validation case. The hill geometry definition is defined by Kim et al. [28], where $SxHy$ denotes a maximum slope of $0.x$ and a height of y. The hill geometry is defined with the following equation

$$y = \frac{H}{2}\left\{1 + \cos\left[\left(\frac{\pi}{2}\right)\left(\frac{x}{L_1}\right)\right]\right\} \quad (24)$$
$$\text{where} \quad L_1 = \frac{H}{2S}$$

Figure 3 shows the geometry modeled with $S = 3$ and $H = 4$. This geometry was chosen because of the severe adverse pressure gradient on the down-wind side. While the flow does stay attached, it is very close to separa-
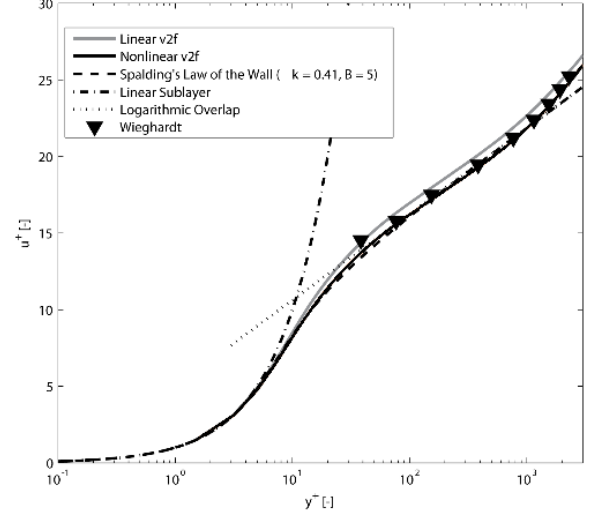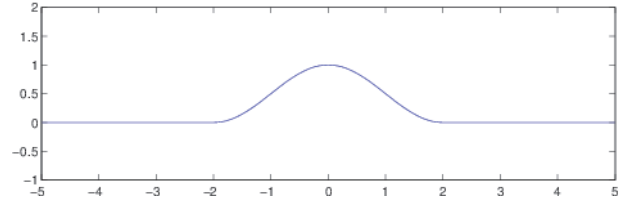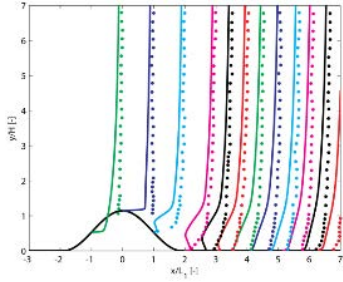

Fig. 3 S3H4 hill geometry from Kim et al. [28].

tion; with a slightly larger hill would result in separation.

Velocity profiles generated with the $v^2 - f$ turbulence models were compared to profiles generated with standard turbulence models and experimental data gathered by Kim et al [28]. These are shown in figure 4. The streamline curvature and potential for separation makes the case an excellent validation case, with the potential to demonstrate an improvement in the nonlinear eddy viscosity.

The experimental data show no separation region downstream of the hill, while the Spalart-Allmaras and linear $v^2 - f$ turbulence models show separation. The $k - \epsilon$, $k - \omega$, and nonlinear $v^2 - f$ turbulence models show no separation, which is consistent with the experimental data.
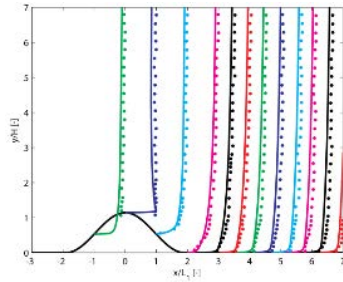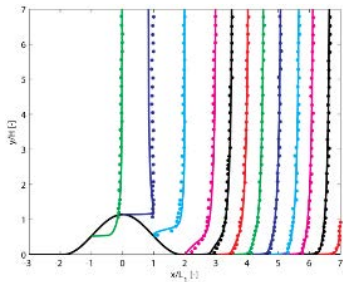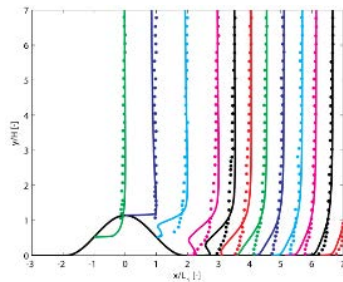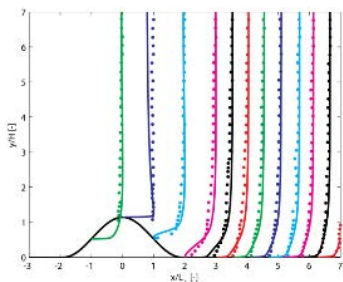
(a) Spalart-Allmaras

(b) $k - \epsilon$

(c) $k - \omega$

(d) Linear $v^2 - f$

(e) Nonlinear $v^2 - f$

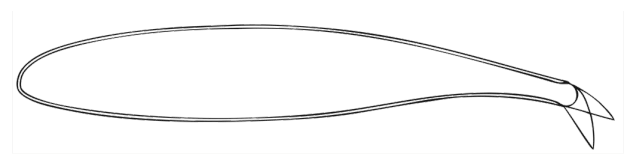**Fig. 4** Velocity profiles at various locations along bump compared to experimental data from Kim et al. [28].

Fig. 5 General aviation circulation control (GACC) airfoil used for this study.

4 Circulation Control Results

The $v^2 - f$ turbulence models were applied to the General Aviation Circulation Control (GACC) airfoil and compared to the results from Jones et al. [29] and Lee-Rausch et al. [8]. Results were also generated using the turbulence models presented by Lee-Rausch et al. and Jones et al. to ensure the mesh and CFD solver are adequate. Figure 5 shows the GACC airfoil geometry. The trailing edge slot is at the start of the flap. The flap is a dual-radius flap geometry.

4.1 Mesh

Careful attention was paid to the grid generation process to limit errors due to poor grid quality. In particular, several aspects of the grid were scrutinized. First, gridline orthogonality needed to be enforced to minimize numerical error. This criterion, along with the large flap deflection, led to a unique farfield configuration; this was necessary to provide adequate mapping of gridlines from both the flap and the near-flap region on the lower surface to the farfield. Second, since the $v^2 - f$ turbulence model does not use damping functions nor wall functions, the cell nearest any wall needed to be placed in the laminar sublayer. The meshing criteria was to ensure that $y^+ < 5$. Third, the leading edge discretization needed to be sufficient to capture the stagnation point, which is crucial in predicting the lift coefficient. Finally, the grid needed sufficient resolution in the wake region to capture any recirculation, should the $v^2 - f$ turbulence model predict it. The slot region needed to be accurately resolved in order to capture the slot
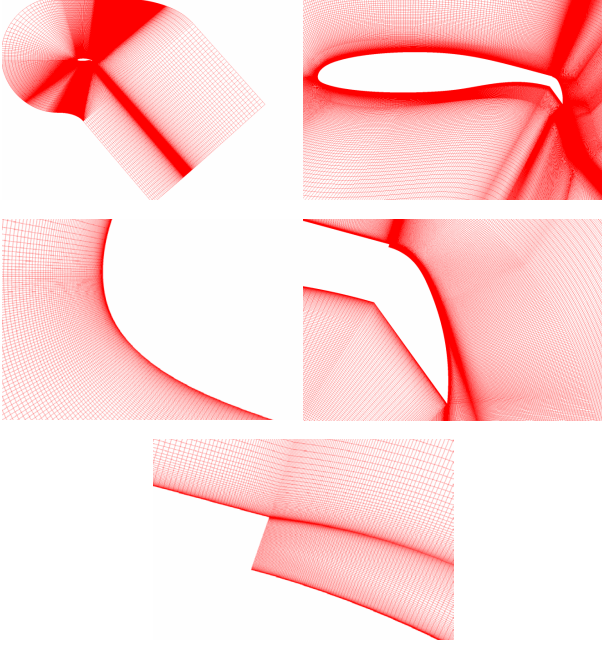
Fig. 6 Views of the computational mesh used in this study of the circulation control airfoil.

flow around the flap. Also, the shear layer between the flow over the upper surface and slot needed to be resolved. A fully structured grid was generated to meet these criteria. The computational grid is shown in figure 6.

4.2   Force Coefficients

Figure 7 shows the lift coefficient variation with respect to the blowing coefficient. The linear and nonlinear $v^2 - f$ turbulence models show improvement in the prediction of the lift coefficient for the GACC airfoil, and the results obtained using common turbulence models showed the same over-prediction that Jones et al. and Lee-Rausch et al. observed. It is worth noting that these data are only for blowing coefficients up to approximately 0.16, while values of 0.50 and higher are not uncommon. In this light, it appears that even the $v^2 - f$ models will over predict the lift coefficient in these higher blowing coefficient cases, however there is no data available to compare against.

Comparing the drag coefficient variation with respect to blowing coefficient, figure 8
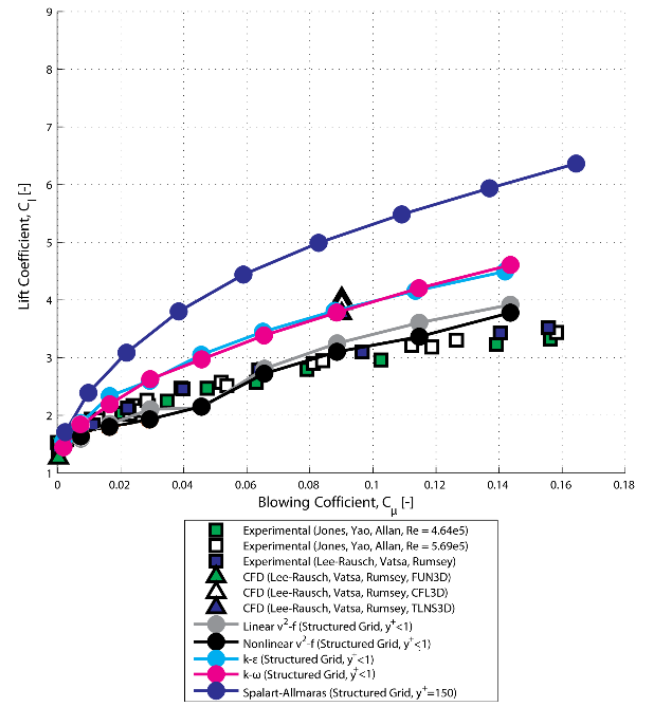

Fig. 7 Lift coefficient variation with respect to slot blowing coefficient for the various turbulence models compared to the computational data from Lee-Rausch et al. [8] and experimental data from Lee-Rausch et al. [8] and Jones et al. [29].
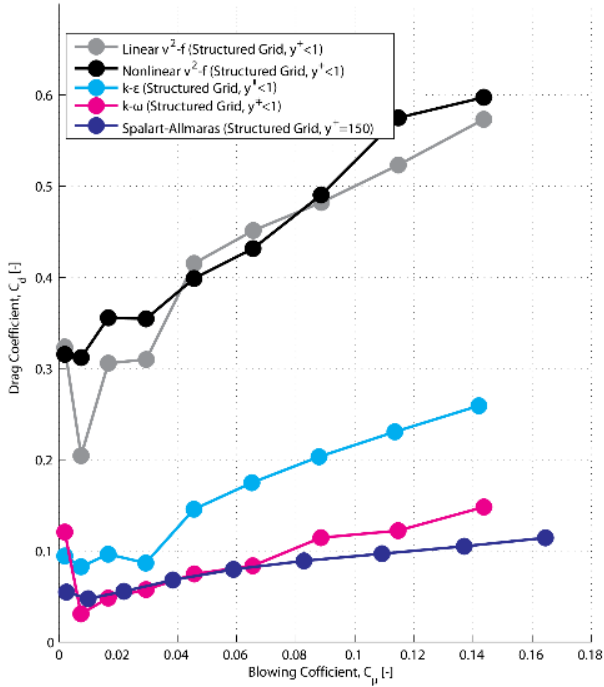
Fig. 8 Drag coefficient variation with respect to slot blowing coefficient for the various turbulence models.

shows there is a significant difference between the $v^2 - f$ data and the other turbulence model data. Again, without experimental data to provide validation, it is difficult to assess the capabilities of any of the turbulence models in predicting drag.

4.3 Surface Quantities

Figure 9 shows the pressure coefficient distributions generated by the standard turbulence models and the $v^2 - f$ turbulence models for the GACC airfoil at a blowing coefficient of 0.084. These data are compared to those presented by Lee-Rausch et al. Results for the linear and nonlinear $v^2 - f$ turbulence models indicate reasonable agreement for the pressure coefficient for most of the airfoil, including the region surrounding the circulation control slot. However, these turbulence models produced significantly lower pressure coefficient than the experimental results and other turbulence models at the suction peak on the upper surface of the leading edge.
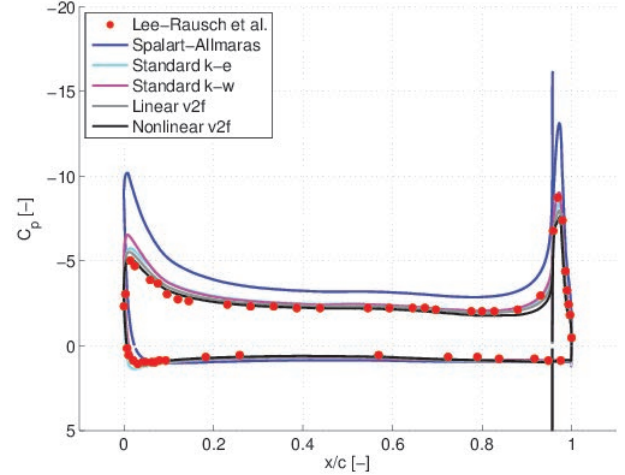

Fig. 9 Pressure coefficient values on the circulation control airfoil for the various turbulence models and experimental data from Lee-Rausch et al. [8] for $C_\mu = 0.084$.

The $v^2 - f$ turbulence models predict the lift coefficient much more accurately than common turbulence models; however, they do not predict the pressure coefficient nearly as accurately. The under prediction of the pressure coefficient near the suction peak contributes primarily to pressure drag rather than lift and may indicate that the drag predictions from figure 8 are over-predicted for the $v^2 - f$ models.

Figure 10 shows the skin friction coefficient predictions for the GACC airfoil at a blowing coefficient of 0.084. The turbulence models used in this comparison predict similar skin friction profiles with the two exceptions. First, the Spalart-Allmaras turbulence model predicts significantly higher skin friction on the leading edge and the upper surface of the flap, shown in figures 11 and 12 respectively. Second, the leading edge skin friction coefficient predictions vary widely between the various turbulence models, noting that the two $v^2 - f$ models do predict similar values. Experimental results for the skin friction profile are not available for the GACC airfoil, therefore any quantitative analysis of the accuracy of the turbulence models predictive capabilities with respect to skin friction is not possible.
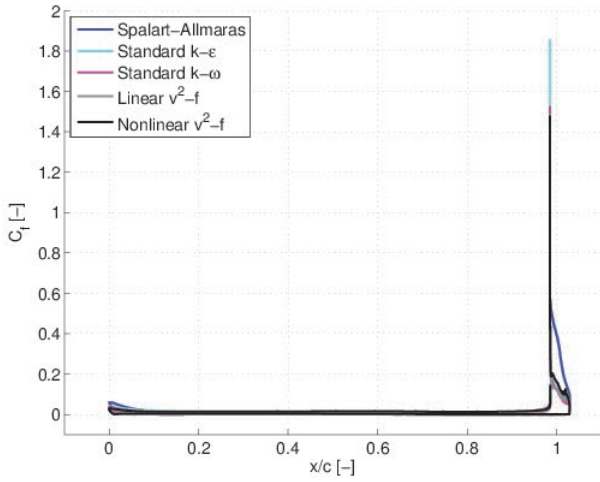
Fig. 10 Skin friction coefficient values on the circulation control airfoil for the various turbulence models for $C_\mu = 0.084$.
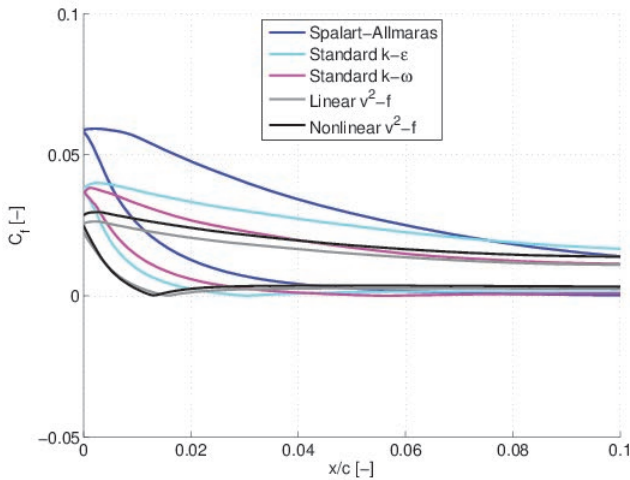

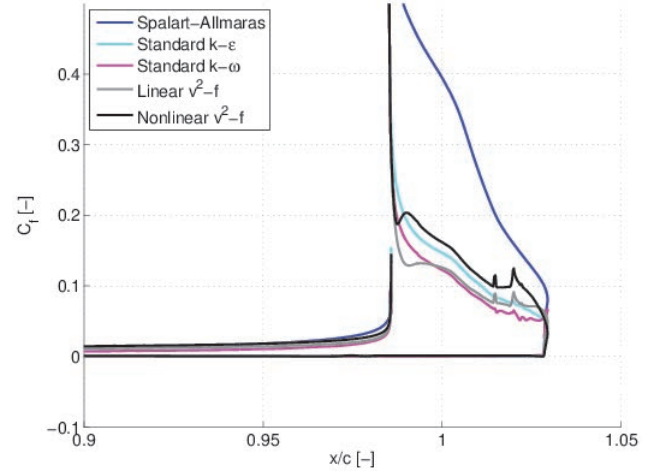**Fig. 12** Trailing edge skin friction coefficient values on the circulation control airfoil for the various turbulence models for $C_\mu = 0.084$.

4.4 Velocity Field

Another quantity that can be compared between the experimental data from Jones et al. and these turbulence models is the velocity field around the airfoil. Jones et al. reported the velocity field around most of the upper surface and along the lower surface just past the forward stagnation point. Figure 13 shows the Jones et al. data and the various turbulence model predictions. Clearly, Spalart-Allmaras and the two two-equation turbulence models are drastically over-predicting the upper surface velocity (thus the over-prediction of lift), while the two $v^2 - f$ models are much closer to the experimental velocity.

Another property that can be compared between the experimental data and the computational data is the location of the forward stagnation point. The experimental data show the forward stagnation point to be at $x/c = 0.03$ while the turbulence models predict a wide variety of locations. While the predicted stagnation point location of the $v^2 - f$ models is reasonably close at $x/c = 0.0115$ and $x/c = 0.0127$ for the linear and nonlinear models respectively, they do not perform much better than the two-equation model predictions.
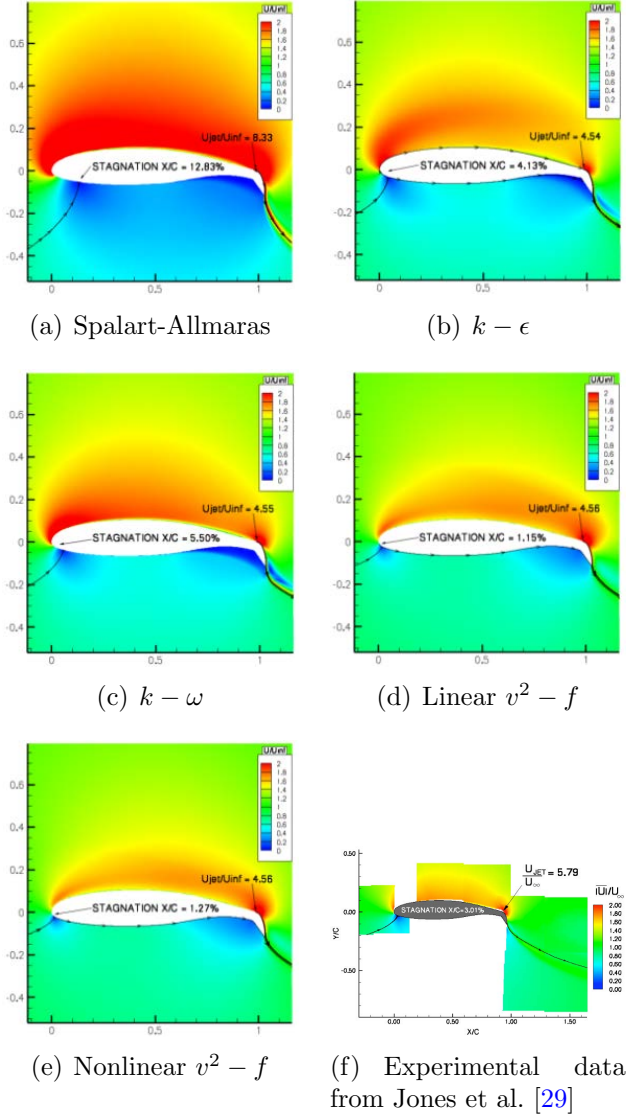

Fig. 11 Leading edge skin friction coefficient values on the circulation control airfoil for the various turbulence models for $C_\mu = 0.084$.

The final data to be compared is the trailing edge flow and is shown in figure 14. This region is significant since the circulation control flow is in this region. Comparing the turbulence model predictions to the experimental data, it is clear that none of the turbulence models do a satisfactory job at capturing the flow accurately. The direction of the slot flow wake coming off of the trailing edge flap is not well predicted. All of the turbulence models except for Spalart-Allmaras drastically over-predict the size of the low-speed region above the slot flow aft of the trailing edge. From this figure, it is clear that there is a significant amount of flow physics that none of these turbulence models are capturing.

5   Conclusions

While the two $v^2 - f$ turbulence models have done a better job of predicting the lift coefficient for a circulation control airfoil flow, there are a number of flow characteristics that are not well captured. In terms of turbulence model capabilities, the $v^2 - f$ models outperformed the other turbulence models in predicting the performance of the GACC, but there is definite room for improvement. The nonlinear eddy viscosity models, and even more sophisticated turbulence models being developed, provide the best chances for improving the predictive capabilities of RANS solvers for circulation control flows.

6   Acknowledgements

(a) Spalart-Allmaras

(b) $k - \epsilon$

(c) $k - \omega$

(d) Linear $v^2 - f$

(e) Nonlinear $v^2 - f$

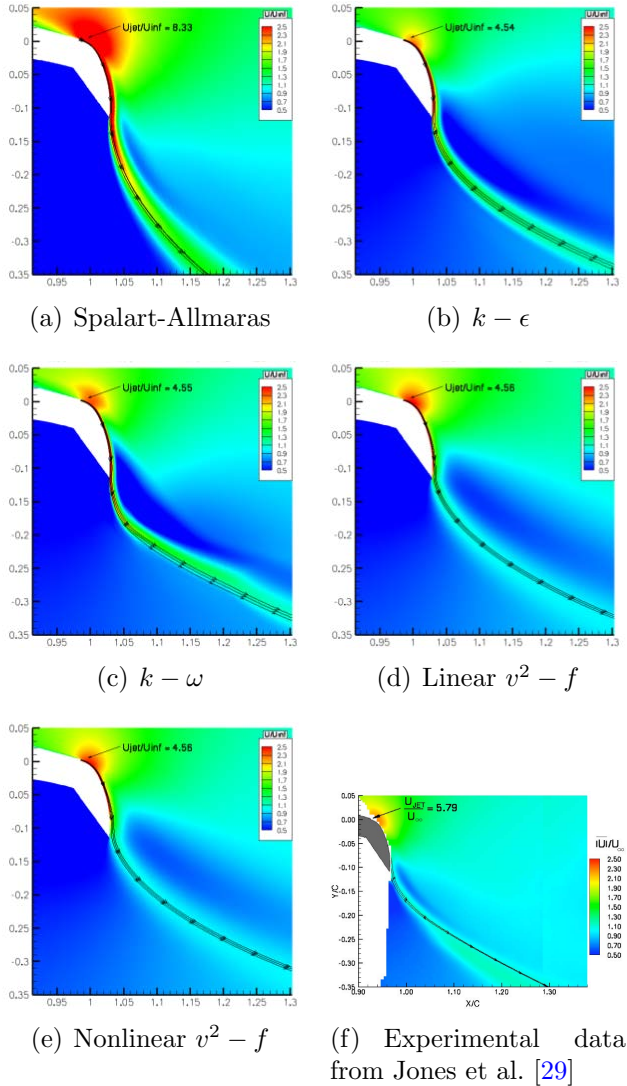(f) Experimental data from Jones et al. [29]

Fig. 13 Velocity contours for the various turbulence models and the experimental velocity contours from Jones et al. [29].

References

[1] Robert J. Englar and Gregory C. Huson. Development of advanced circulation control wing high-lift airfoils. *Journal of Aircraft*, 21(7):476–483, July 1984.

[2] T. Panitz and D. T. Wasan. Flow attachment to solid surfaces: the coanda effect. *American Institute of Chemical Engineering Journal*, 18(1), 1972.

[3] L. Jingchang, S. Mao, and W. Liyi. Navier-Stokes analysis of a circulation control airfoil. *ACTA Mechanica Sinica*, 11(2), 1995.

[4] Y. Liu. *Numerical Simulation of the Aerodynamic Characteristics of Circulation Control Wing Sections*. PhD thesis, Georgia Institute of Technology, Atlanta, GA, 2003.

[5] Y. Liu, Lakshmi N. Sankar, Robert J. Englar, and K. K. Ahuja. Numerical simulation of the steady and unsteady characteristics of a circulation control wing airfoil. In *39th Aerospace Sciences Meeting and Exhibit*, Reno, NV, January 2001. AIAA. AIAA-2001-0704.

[6] Gregory McGowan and Ashok Gopalarathnam. Computational study of circulation control airfoil using FLUENT. In Ronald D. Joslin and Gregory S. Jones, editors, *Applications of Circulation Control Technology*, volume 214 of *Progress in Astronautics and Aeronautics*, chapter 21, pages 539–554. American Institute of Aeronautics and Astronautics, Inc., 2006.

[7] Tyler Matthew Ball. CFD as applied to the design of short takeoff and landing vehicles using circulation control. Master's thesis, California Polytechnic State University, San Luis Obispo, CA, June 2008.

[8] E. M. Lee-Rausch, V. N. Vatsa, and Christopher L. Rumsey. Computational analysis of dual radius circulation control airfoils. In *36th Fluid Dynamics Conference*, San Francisco, CA, June 2006. AIAA. AIAA-2006-3012.

[9] R. C. Swanson, Christopher L. Rumsey, and S. G. Anders. Progress towards computational method for circulation control airfoils. In *43rd AIAA Aerospace Sciences Meeting and Exhibit*, Reno, NV, January 2005.

(a) Spalart-Allmaras (b) $k - \epsilon$

(c) $k - \omega$ (d) Linear $v^2 - f$

(e) Nonlinear $v^2 - f$ (f) Experimental data from Jones et al. [29]

Fig. 14 Velocity contours for the various turbulence models and the experimental velocity contours from Jones et al. [29].

AIAA. AIAA-2005-0089.

[10] P. Chang, J. Slomski, T. Marino, and M. P. Ebert. Numerical simulation of two- and three-dimensional circulation control problems. In *43rd AIAA Aerospace Sciences Meeting and Exhibit*, Reno, NV, January 2005. AIAA. AIAA-2005-0080.

[11] Gregory McGowan, Ashok Gopalarathnam, and S. Jones. Analytical and computational study of adaptive circulation control airfoils. In *22nd AIAA Applied Aerodynamics Conference*, Providence, RI, August 2004. AIAA. AIAA-2004-4721.

[12] A. M. O. Smith and Tuncer Cebeci. Numerical solution of the turbulent boundary layer equations. DAC 33735, Douglas Aircraft Division Report, 1967.

[13] Barrett Baldwin and Harvard Lomax. Thin layer approximation and algebraic model for separated turbulent flows. In *16th AIAA Aerospace Sciences Meeting*, Huntsville, AL, January 1978. AIAA. AIAA-78-257.

[14] P. R. Spalart and S. R. Allmaras. A one-equation turbulence model for aerodynamic flows. In *30th AIAA Aerospace Sciences Meeting*, Reno, NV, January 1992. AIAA. AIAA-92-0439.

[15] B. E. Launder and D. B. Spalding. *Lectures in Mathematical Models of Turbulence*. Academic Press, Inc., London, England, 1972.

[16] David C. Wilcox. *Turbulence Modeling for CFD*. DCW Industries, Inc., second edition, 1994.

[17] Paul A. Durbin. Near-wall turbulence closure modeling without "damping functions". *Theoretical and Computational Fluid Dynamics*, 3(1):1–13, September 1991.

[18] S. B. Pope. A more general eddy-viscosity hypothesis. *Journal of Fluid Mechanics*, 72:331–340, 1975.

[19] Br. Bell. Turbulent flow case studies. Technical report, Fluent Services Center, 2003.

[20] S. Parneix, Paul A. Durbin, and M. Behnia. Computation of 3-D turbulent boundary layers using the V2F model. *Flow, Turbulence, and Combustion*, 60, 1998.

[21] M. Behnia, S. Parneix, and Paul A. Durbin. Prediction of heat transfer in a jet impinging on a flat plate. *International Journal of Heat and Mass Transfer*, 41, 1998.

[22] B. A Petterson Rief. A nonlinear constitutive relationship for the $v^2 - f$ model. Annual research briefs, Center for Turbulence Research, 1999.

[23] Travis M. Storm. Assessing the v^2-f turbulence models for circulation control applications. Master's thesis, California Polytechnic State University, San Luis Obispo, CA, April 2010.

[24] C. Heschl, W. Sanz, P. Klanatsky, and F. Madou. Comparison of different turbulence models to compute wall affected room airflows. Technical report, TU Graz, Institute for Turbomachinery and Machine Dynamics, 2005.

[25] C. Heschl, W. Sanz, P. Klanatsky, and F. Madou. Implementation and comparison of different turbulence models for three dimensional wall jets with FLUENT. Technical report, TU Graz, Institute for Turbomachinery and Machine Dynamics, 2005.

[26] Frank M. White. *Viscous Fluid Flow*. McGraw-Hill Series in Mechanical Engineering. McGraw-Hill, New York, NY, second edition, 1991.

[27] K. Wieghardt and W. Tillmann. On the turbulent friction layer for rising pressure. Technical Memorandum 1314, National Advisory Committee for Aeronautics, Washington, DC, October 1951.

[28] Hyun Goo Kim, Choung Mook Lee, H. C. Lim, and N. H. Kyong. An experimental and numerical study of the flow over two-dimensional hills. *Journal of Wind Engineering and Industrial Aerodynamics*, 66(1):17–33, January 1997.

[29] Gregory S. Jones, Chung-Sheng Yao, and Brian G. Allan. Experimental investigation of a 2D supercritical circulation-control airfoil using particle image velocimetry. In *36th Fluid Dynamics Conference*, San Francisco, CA, June 2006. AIAA. AIAA-2006-3009.

Copyright Statement

original material included in this paper. The authors also confirm that they have obtained permission, from the copyright holder of any third party material included in this paper, to publish it as part of their paper. The authors confirm that they give permission, or have obtained permission from the copyright holder of this paper, for the publication and distribution of this paper as part of the ICAS2012 proceedings or as individual off-prints from the proceedings.